Submission code: GDZK6VZJAB

See this and other abstracts on our website: https://home.sbgf.org.br/Pages/resumos.php

Towards more accurate interpretation of seismic images with Elastic Full Waveform Inversion (EFWI)

Jaime Ramos-Martinez (TGS), Faqi Liu (TGS), Guanghui Huang (TGS), Cosmin Macesanu (TGS), Dan Whitmore (TGS), James Sheng (TGS), Carlos Calderon (TGS)

Towards more accurate interpretation of seismic images with Elastic Full Waveform Inversion (EFWI)

Abstract

One of the most significant improvements in model building and seismic imaging has been the incorporation of elastic wave propagation in full waveform inversion. We have extended Dynamic Matching Full Waveform Inversion (DM FWI) from acoustic to elastic medium resulting in FWI images that are structurally better focused with a higher resolution compared to the acoustic version. This approach has been mostly a single parameter inversion that focuses on inverting the P wave velocity through frequency staging, thus reflectivity is derived by utilizing the derivative in the orthogonal direction to the structure from the inverted velocity. Recently, we developed an elastic FWI approach that jointly inverts the background P-wave velocity and the reflectivity by separating the wavelength scales in the gradient to minimize parameter crosstalk. We have applied these approaches to sparse Ocean Bottom Node (OBN), and to streamer data with improved results versus the acoustic implementations. These methods can be cascaded for a robust estimation of properties. In this paper, we discuss the algorithms and demonstrate the benefits of their application with field data results.

Introduction

Since the original proposition of Full Waveform Inversion (FWI) for model building (Tarantola, 1984), many developments have significantly advanced the technology. These improvements can be broadly categorized in enhanced robustness of the algorithms, cycle skipping mitigation to avoid local minima, optimization approaches to improve convergence, model regularization and augmented physics. These have also been coupled with advancements in seismic acquisition including surveys with ultra-long offsets, full azimuth and the use of marine sources that extend the frequency bandwidth towards low and ultra-low end. The net effect is an increase in image resolution and a reduced uncertainty of the inverted model contributing to reservoir characterization. To manage cost, sparse node acquisition and simultaneous shooting have become common practices. While this type of acquisition has proved a high cost-benefit ratio, high resolution imaging has relied on a tighter spatial sampling of small angles.

The successful application of acoustic FWI to sparse OBN data has been documented in several publications (e.g., Huang et al., 2023). DM FWI relies on maximizing the match between the field and synthetic data to construct extract a high-resolution velocity model that predicts the observed data. This method has been recently extended to the elastic case (Liu et al., 2025). The enhancement in physics enables to produce a better match to the field data in the presence of high impedance contrasts such as salt boundaries, especially at relatively shallow targets. This also applies to any case where wave propagation with the acoustic assumption deviates from the elastic response, such as the presence of amplitude anomalies in AVO studies. In the work of Liu et al. (2025), the compressional velocity, v_p, is inverted, while density and shear wave velocity, ρ and v_s, are respectively estimated through empirical information with well constraints, where such information is available. After frequency staging, FWI Image or FWI derived reflectivity (FDR), is obtained directly from the velocity field by computing a spatial derivative in the orthogonal direction to the dip of the reflector.

Alternatively, in a multiparameter (MP) elastic FWI, the P-wave reflectivity can be jointly inverted with the P-wave velocity (Huang et al., 2025). This method is based on a reformulation of the elastodynamic wave equation in terms of P-wave reflectivity instead of density. In contrast with the use of an empirical density model, the reflectivity is determined from the surface seismic data. Furthermore, the initial reflectivity is updated within the FWI framework. Accordingly, the other key element is the scale separation of the FWI gradient to reduce crosstalk between background velocity and reflectivity during the inversion.

In this work, we discuss single and multiparameter elastic FWI implementations with the dynamic matching cost function. We illustrate the benefits of these approaches with field data examples.

Methods

The elastic FWI with the dynamic matching (DM) cost function is described in the works by Macesanu et al. (2024) and Liu et al. (2025). This cost function aims to maximize the phase match between the recorded and synthetic data using a multidimensional cross-correlation. This allows a significant reduction in the

sensitivity to noise and amplitude mismatch effects during the inversion. For the single parameter elastic inversion, the starting velocity model is generally obtained from a smoothed version of a legacy model or from low-resolution reflection tomography. The initial density and S-wave velocity models are computed from P-wave velocity using empirical relations and well log information where is available. The inversion focuses on inverting P wave velocity, while the other two parameters (density and S-wave velocity) are updated passively using the empirical relations.

The theory of the MP elastic FWI for jointly invert for P-wave velocity and reflectivity is explained in detail in Huang et al. (2025). One of the motivations of the approach is to use reflectivity rather than density, a parameter that is difficult to determine from surface seismic data (Whitmore 2020). The elastodynamic equation provides a seismic response equivalent to that provided by the conventional formulation. The P-wave reflectivity is updated using the same FWI framework. As in the acoustic case (Yang et al., 2021), the joint inversion mitigates the crosstalk between the background P-wave velocity and the reflectivity. This is achieved for the elastic case, following a similar procedure based on scale separation in the FWI gradient described by Whitmore and Crawley (2012) and Ramos-Martinez et al. (2015).

To illustrate the significance of the enhancement in physics, in Figure 1 we compare the sensitivity kernels for velocity and reflectivity for the elastic DM FWI and their equivalent assuming acoustic propagation. These sensitivity kernels were computed from an intermediate angle trace corresponding to the elastic response for a Class II AVO anomaly, as shown in Figure 1a. For comparison, the acoustic response is shown in Figure 1b. Figures 1c and 1e show the velocity and reflectivity kernels computed from the elastic DM FWI . In Figures 1d and 1f, we show the kernels computed from acoustic propagation. Notice the phase variation of the velocity kernels when inaccurate physics are utilized in the acoustic result (Figure 1d). These phase differences can also be observed in the acoustic propagation, when density is assumed to positively correlate with the velocity contrast at the interface.

Field data examples

OBN examples

We applied acoustic and elastic single parameter FWI to a sparse OBN data from the Gulf of Mexico. The data was acquired with a maximum offset of 45 km, and receivers were sparsely placed on the ocean floor at 1.2 km intervals in both horizontal directions. Two source vessels with triple sources each were combined to allow for the recording of low frequency signal below 2 Hz. The hydrophone data after debubble and basic denoise was used as input to acoustic and elastic FWI up to a maximum frequency of 12 Hz. The final velocity models and the corresponding FWI images are shown in Figure 2. Compared to acoustic DMFWI (Figure 2a), elastic DMFWI simulates more accurately the phase and amplitude of the wavefield, which results in reduced salt halos, sharper salt boundaries, better defined salt feeders and enhanced definition of geological inclusions. Notably, the elastic DMFWI image (Figure 2b) offers significant improvements in areas with poor illumination beneath salt.

The second example shows the application of the multiparameter approach to a OBN data in deep-water Santos Basin, offshore Brazil. This dataset consists of 954 nodes covering an area of approximately 111 km^2 with sources covering about 345 km^2. FWI was performed starting at 2 Hz and up to the maximum of 25 Hz using data with minimal pre-processing. In Figure 3, we show the comparison of an inline and a depth section, with panels a) and c) showing the inverted velocity model and reflectivity from the multiparameter acoustic inversion, and panels b) and d) display the same corresponding sections from the elastic inversion. The acoustic algorithm produces a less focused boundary at the top of the salt with spurious variations in velocity at the interface. Consequently, the inverted reflectivity exhibits a less defined salt boundary (Figure 3c). In contrast, the elastic algorithm produces a more focused boundary in velocity with a higher resolution at the top of the salt (Figure 3b). Likewise, the inverted reflectivity corresponding to the elastic case shows enhanced resolution for the salt boundary (Figure 3d). Figures 3e and 3f compare a depth slice of the two inverted reflectivity models, where the elastic result in Figure 3f clearly shows a more focused image and improved resolution at the salt boundary. Note, in multi-parameter DM FWI, the reflectivity is directly inverted from the data and the velocity model contains only long wavelength components that control the kinematics while the short wavelength portion appears in the reflectivity.

Narrow azimuth streamer example

The third example corresponds to streamer data also acquired in deep-water offshore Brazil. In this geological setting located in the Sergipe-Alagoas basin. The water depth ranges between 1500 to 3200 m. The data were acquired with a narrow azimuth survey using a 12-cable configuration with a maximum inline offset of 8100 m. As in the OBN data examples, we applied minimal preprocessing comprising basic denoise and debubble. The maximum frequency in the inversion is 25 Hz. The initial P-wave velocity model was built from reflection tomography. The initial S-wave model is computed from an empirical relation. The reflectivity model is constructed and refined within the inversion frame. In Figure 4a, we show the RTM image overlaying the initial P-wave velocity model from tomography. In Figure 4b, we show the inverted reflectivity overlaying the inverted background velocity using the elastic multiparameter FWI. A significant uplift in resolution is observed from the inverted reflectivity compared to those of the conventional imaging workflow. Reflectors below the high-impedance volcanic plugs in the basin show enhanced continuity and resolution for the inverted reflectivity. Figures 4c and 4d compare one depth slice of the RTM image using the initial velocity and the inverted reflectivity. There is a significant improvement in the resolution of the inverted reflectivity comprising enhanced fault delineation and sharpening of the high-impedance contrast events.

Conclusions

We show that Elastic FWI produces sharper images than those obtained from acoustic FWI in geological settings with the presence of complex salts bodies or volcanic rocks. This success has been explained as a more accurate description of the physics in wave propagation where phase variations due to density and shear-wave velocity contrasts may occur. Most successful case studies have resulted from OBN acquisitions, while success with streamer data has been reported less. This might be due to the limitations of reflection angles which tend to be narrower, especially in steep dips. We present elastic FWI results with single and multiparameter FWI approaches, superior to the acoustic counterpart of these methods. The implementation of the multiparameter inversion method reduces parameter crosstalk, resulting in a reflectivity image with reduced artifacts.

Acknowledgments

We thank TGS for permission to publish this material and TGS Muticlient for providing the datasets used in this work. We thank our colleagues Hao Xing and Richard Huang for producing the Amendment results as well as Alejandro Alcudia-Leon and Eric Frugier for their assistance in the data preparation for the Brazil results.

References

Huang, Y., Mao J., Sheng, J., Perz, M, He, Y., Hsao, F., Liu, F., Yong, S.L., Chaikin, D, Ramirez, A, Hart, M. and Roende, H. [2023]. Towards high-fidelity imaging: Dynamic Matching FWI, TLE, 42, 124-132.

Huang, G., Macesanu, C., Liu, F., Ramos-Martinez, J., Whitmore and Calderon, C [2025]. Multiparameter elastic FWI for joint inversion of velocity and reflectivity, 86th *EAGE Conference and Exhibition, Extended Abstracts.*

Macesanu, C., Liu, F., Huang, Y., Mao, H. and Calderon, C. [2024] Implementation aspects of elastic FWI and its application to sparse OBN data. *Fourth International Meeting for Applied Geoscience and Energy, Expanded Abstracts*, 886-890.

Liu, F., Macesanu, C., Hu, H., Romanenko, M., Zhan, G., Calderon C. and Wang B, [2024], Elastic full-waveform inversion: Enhance imaging for legacy and modern acquisition, TLE, 44, 338-343.

Ramos-Martinez, J., Crawley, S., Zou, K., Valenciano, A.A., Qiu, L. and Chemingui, N. [2016] A robust gradient for long wavelength FWI updates, *78th EAGE Conference & Exhibition,* Extended Abstracts.

Whitmore, N.D., Ramos-Martinez, J., Yang Y. and Valenciano, A.A. [2020] Full wave field modelling with vector-reflectivity, *82nd EAGE Conference & Exhibition,* Extended Abstracts.

Whitmore, N D and Crawley, S. [2012]. Application of RTM inverse scattering imaging conditions, 82nd Annual International Meeting*, SEG Expanded Abstracts*

Yang, Y., Ramos-Martinez, J., Whitmore, D., Guanghui, H. and Chemingui, N. [2021] Simultaneous inversion of velocity and reflectivity. *First Break*, 39(12), 55-59.

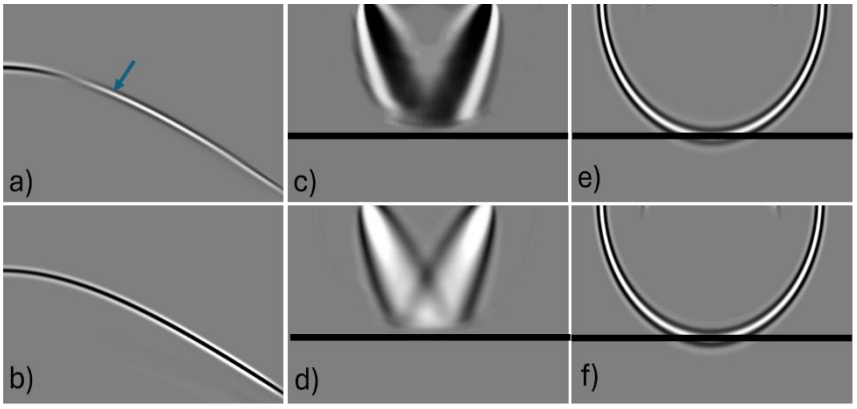

Figure 1 Seismic responses for a two-layer model using a) elastic and b) acoustic propagation. P-wave velocity sensitivity kernels computed for an intermediate angle corresponding to the trace pointed by the arrow using c) elastic and d) acoustic propagation; the corresponding P-wave reflectivity kernels are shown in e) and f) for the elastic and acoustic propagation, respectively.

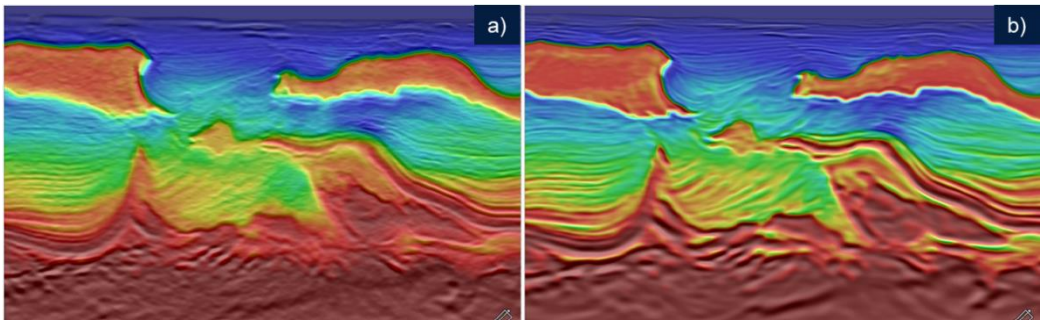

Figure 2. Gulf of Mexico OBN data: a). Velocity model of 12Hz acoustic DMFWI overlaying the corresponding FWI Image and b) Velocity model of 12Hz elastic DMFWI overlaying the corresponding FWI Image.

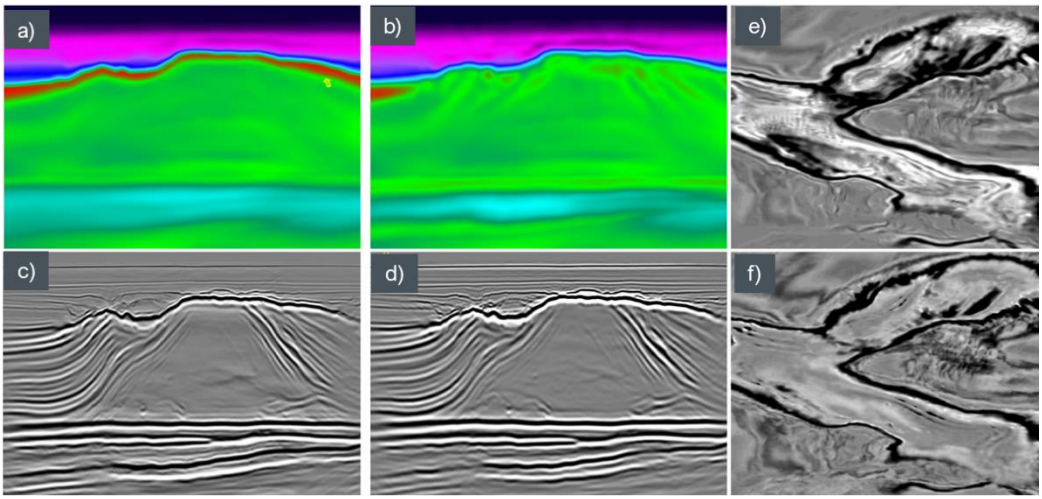

Figure 3. Santos basin MP FWi example: One inline of the inverted a) velocity and c) reflectivity models using the acoustic MP FWI algorithm. The corresponding line of the inverted b) velocity and d) reflectivity models using the elastic MP FWI algorithm. Depth slice of acoustic (e) and elastic inversion (f).

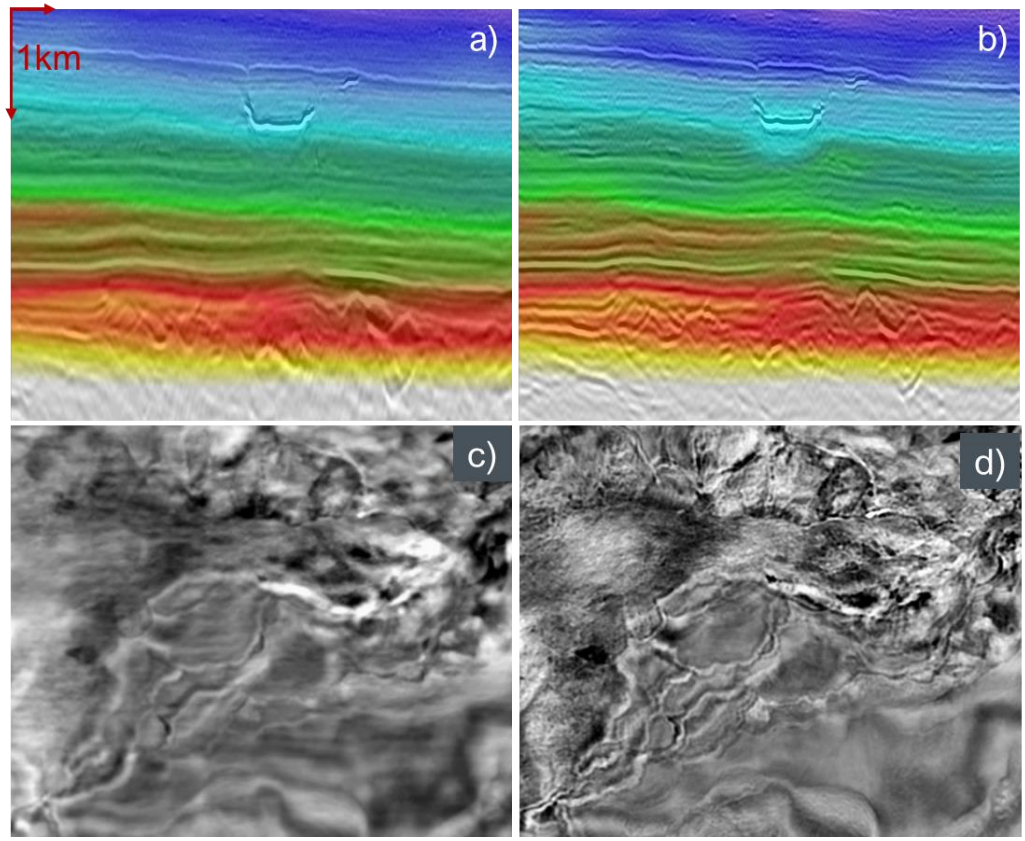

Figure 4. MP FWI example of narrow azimuth data. a) RTM image overlaying the initial velocity model; b) inverted reflectivity overlaid on the inverted background model from the MP elastic approach. Depth slices for the c) conventional RTM image using preprocessed data and the d) inverted reflectivity using MP elastic FWI algorithm.